

Chronological Calibration Methods for Landsat Satellite Images

S.M. Ali¹, S.S. Salman²

^{1&2} University of Baghdad, Iraq, Baghdad, Al- Jaderyia

¹ College of Science, Department of Remote Sensing, ² College of Pharmacy

Abstract : Because of the rapid growth in agricultural yields plants and the temporal variation of satellite pass over the fields (e.g. 8-days repeat coverage between Landsat 7&8), and for the purpose of accuracy in estimating the amount of the expected crop yields that can be obtained by utilizing different satellite's images. The present research introduces a chronological calibration method for individual satellite image bands. Gaps bridging method based on the neighborhood is used to correct the failure of Scan Line Corrector (SLC) occurred in ETM+ images. The Landsat images are corrected by converting their density values to Top of Atmosphere (ToA) reflectance. Two methods have been suggested to remove the effects of phenology within the 8-days interval between Landsat 7 and 8 images; i.e. utilizing the linear regression equation and the cross-correlation-factor. Image classification method based on scatterplot between the Visible Red (VR) and Near Infrared (NIR) bands is used to validate the application of these correction methods, by comparing the detected rates of Landcover components in images of the study area.

Keywords: ETM+ SLC Gap filling, Atmospheric correction, Landsat chronological calibration, Scatterplot classification.

I. Introduction

Since 1982 the Landsat series has been lunched to observe the Earth's surface. In 1999 the Landsat-7 was lunched which carry the Enhancement Thematic Mapper Plus (ETM+) instrument starts providing images of the land surface, continuously, in six difference wavelength bands, with spatial ground resolution of 30m. [1]. The Scan Line Corrector (SLC) of the ETM+ sensor has been undergoing a failure since 31 May 2003. Despite the fact that each ETM+ SLC-off scene misses about 22% of the data, these images remained representing one of the most important remotely sensed data for many researchers [2]. On 11 February 2013, the next in the Landsat series was launched. Initially known as the Landsat Data Continuity Mission (LDCM), it was placed in its operational orbit on 12 April 2013. Landsat-8 carries a new instrument called the Operational Land Imager (OLI), which designed to be continuous with ETM+ and attempts to improve the instrument slightly. In particular, the OLI bands in the near infrared wavelengths have been narrowed significantly, to avoid some atmospheric attenuation effects, which should provide for measurements which are much less affected by atmospheric variation, notably water vapor [3]. Landsat 8 carries two push-broom instruments: the **Operational Land Imager (OLI)**, and the **Thermal Infrared Sensor (TIRS)**. The spectral bands of the OLI sensor, while similar to Landsat 7's ETM+ sensor, provides enhancement from prior Landsat instruments, with the addition of two new spectral bands: a **deep blue visible channel** (band 1) specifically designed for water resources and coastal zone investigation, and a **new infrared channel** (band 9) for the detection of cirrus clouds. A new quality assurance band is also included to provide information on the presence of features such as clouds, water, and snow. Fig.1 shows the band pass wavelengths for Landsat-8 OLI and TIRS sensors compared to Landsat-7 sensors (http://landsat.usgs.gov/lcdm_vs_previous.php). The major properties of the Landsat-8 OLI and TIRS image bands compared with the ETM+ image bands are given in Table-1.

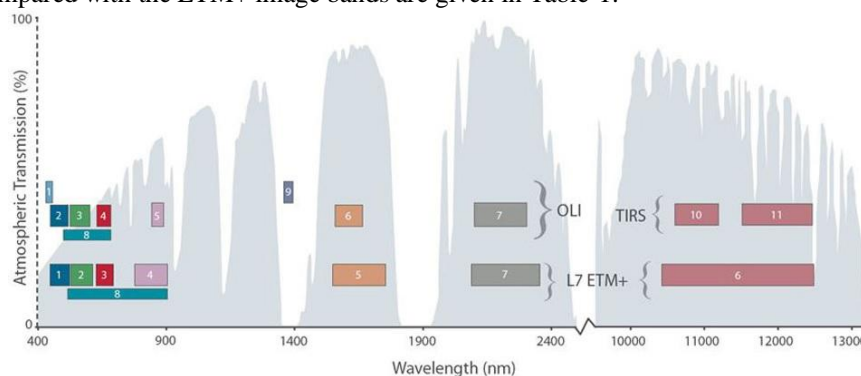


Fig.1: The bands pass wavelengths for Landsat-8 OL107I and TIRS sensors compared to Landsat-7 sensors

Table-1: Comparison of Landsat-7 ETM+ and Landsat-8 OLI/Thermal Infrared Sensor (TIRS) spectral bands (http://landsat.usgs.gov/band_designations_landsat_satellites.php)

Landsat-8 OLI and TIRS		Landsat-7 ETM+		
Bands	Wavelength (µm)	Bands	Wavelength (µm)	Resolution (m)
Band 1—Coastal aerosol	0.43–0.45	NA	-	30
Band 2—Blue	0.45–0.51	Band 1	0.45–0.52	30
Band 3—Green	0.53–0.59	Band 2	0.52–0.60	30
Band 4—Red	0.64–0.67	Band3	0.63–0.69	30
Band 5—Near infrared(NIR)	0.85–0.88	Band 4	0.77–0.90	30
Band 6—Short-wave infrared(SWIR 1)	1.57–1.65	Band 5	1.55–1.75	30
Band 7—Short-wave infrared (SWIR 2)	2.11–2.29	Band 7	2.09–2.35	30
Band 8—Panchromatic	0.50–0.68	Band 8	0.52–0.90	15
Band 9—Cirrus	1.36–1.38	NA	--	30
Band 10—Thermal infrared (TIRS) 1	10.60–11.19	Band 6	10.40–12.50	TIRS/ETM+:
Band 11—Thermal infrared (TIRS) 2	11.50–12.51			100/60 *(30)

The orbits of Landsat-7 and Landsat-8 are such that they alternately revisit each path 8 days apart. This short period of time can cause little change in certain components of the Earth's surface, but for the purpose of monitoring the vegetation growth it may represent a significant difference in vegetative components and lead to wrong estimation of the amount of the expected yield productivity. For this reason, we will try in our present research to harmonize the images captured at different times to get the best estimate of the amount of the expected yield from different satellites images.

Two methods will be tried in this research to harmonize satellite images of specialized rice cultivation area in the southern sector of the Iraq country. The methods will be based on utilizing regression equation and cross correlation factor. Image classification method based on employing the scatterplot between the visual red (VR) and near infrared (NIR) bands to illustrate the improvement in the estimate of the amount of the expected yield of the rice farms in the study area.

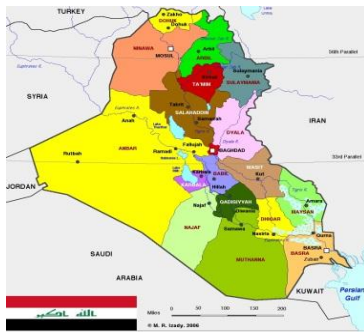
II. Study Area And Data

The *Mashkhab* district is a fertile mudslides land area, about 30 km south of *Najaf* province, 230 km southwest of the *Baghdad* (capital of *Iraq*). A river (called Al-Hidia) of length 25km, which is part of the *Euphrates* River passes through it. As illustrated in Fig.2, the Mashkhab district is located between a number of Iraqi provinces (i.e. Babylon, Karbala, Diwaniya, and Anbar).

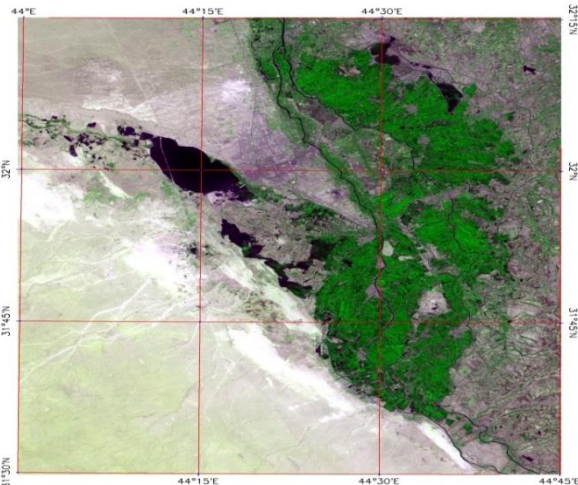


Fig.2: Illustrates the location of the Mashkhab district.

Fig.3 shows the Iraqi administrative map and a photomap (ETM+ color image) representing the study area. The images used in this study are ETM+ captured at 23 September 2014, and OLI at 15 September 2014, which were downloaded from the U.S. Geological Survey (USGS) website. All adopted images taken during the maximum growing season of vegetative growth.



Administrative map of Iraq showing the international and local borders between the provinces. The country lies between the geographic coordinates lat. 37.38° → 28.5° N, and Long. 38.70° → 48.75° E.



Photomap of the study area *Al-Mashkhab* district, Located in the *Najaf* province in the middle-south of Iraq, Lat. 32.25° → 31.5° N, and Long. 44° → 44.75° E.

Fig.3: Administrative map of Iraq country and photomap of the study area.

III. Satellite Image Correction Methods

The following processes will be used to prepare the satellite images and use them in the present research.

A. SLC Restoration of ETM+ Images

The main source which has been adopted in this research to get multispectral band images for the study area was from the *USGS Global Visualization Viewer of the Earth Resources and Science Center (EROS)* [<http://glovis.usgs.gov/>]. It is worth to indicate that the actual location of the study area is located on Path/Row (168/38), and because the presence of gaps due to the failure of *Scan Line Corrector (SLC)* occurred on May 31, 2003, the ETM+ images after May 31, 2003 have been greatly affected by the failure and have lost approximately 22% of their data, appear as gaps, as illustrated in Fig.4.

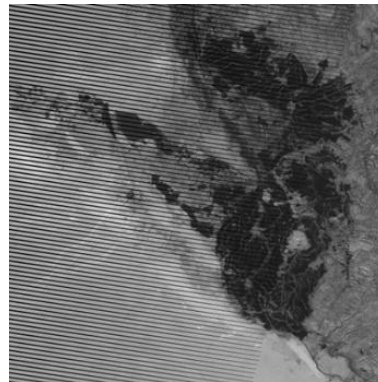


Fig.4: Extracted ETM+ image (with gaps) of the study area taken in 23-09-2014.

A number of digital techniques have been introduced to bridge the gaps in ETM+ images [3]. The majority of the introduced methods used two scenes (taken at different times) to bridge the gaps by transferring pixel values from the undistorted areas of the assisted image to corresponding gap locations in the processed (reference) image. Since the corrected images are required to predict the amount of crop yield, which are subject to change in short periods of time, and because the difficulty in obtaining ETM+ scenes taken in a short interval of time, so in our current research we have adopted gaps bridging methods based on the neighborhood to estimate the gap's values. Two methods have been adopted; i.e.

- The gaps locations were filled by the median value, utilizing large neighborhood window (size 11×11 pixels), the result is illustrated in Fig.5.
- In the second method replaced the gaps by using Delaunay triangulation method to fill the bad pixels with triangles calculated from the surrounding good values [4]. The result is illustrated in Fig.6.

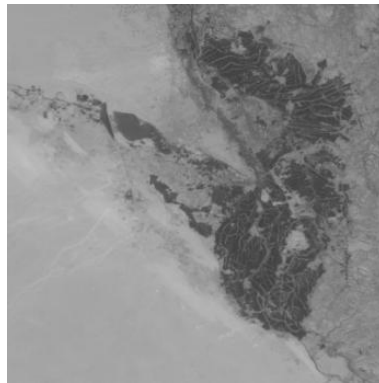


Fig.5: Restored image of study area by median filter of window's size 11×11 pixels

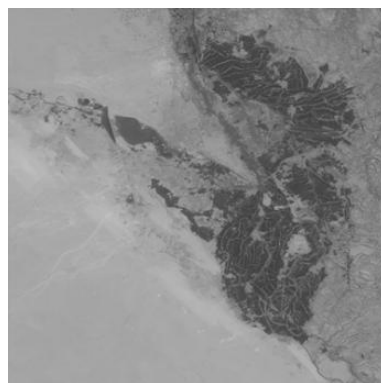


Fig.6: Restored image of study area by replacing the bad (zero) values

B. Converting Landsat DNs to Top of Atmosphere (ToA) Reflectance

The Landsat-7 sensors capture reflected solar energy, convert them to radiance, and then rescale those data into an 8-bits digital number "DN" (range from 0 → 255), while the Landsat-8 sensors rescale the radiance into 16-bits (range from 0 → 65536). The OLI band data can be converted to TOA planetary reflectance using reflectance rescaling coefficients provided in the product metadata file (MTL file) by (http://landsat.usgs.gov/Landsat8_using_product.php). The following equation is used to calibrate DN values to TOA reflectance for OLI data as follows [5]:

$$\rho_{\lambda} = \frac{M_{\rho} Q_{cal} + A_{\rho}}{\cos(\theta_{SZ})} \quad (1)$$

Where: ρ_{λ} = TOA planetary reflectance, M_{ρ} = Bandspecific multiplicative, A_{ρ} = Bandspecific additive, Q_{cal} = Quantized and calibrated standard product pixel values (DN), θ_{SZ} = Local solar zenith angle; $\theta_{SZ} = 90^{\circ} - \theta_{SE}$ where θ_{SE} = Local sun elevation angle.

The Landsat-7 band data can also converts to TOA, using the following calibration equation [6]:

$$\rho_{\lambda} = \frac{\pi L_{\lambda} d^2}{ESUN_{\lambda} \cos(\theta_{SZ})} \quad (2)$$

Where: L_{λ} = Spectral radiance at the sensor's aperture, d = Earth–Sun distance, $ESUN_{\lambda}$ = Mean exoatmospheric solar irradiance, and θ_{SZ} as defined in Eq. (1).

Fig.7 shows samples of ETM+ and OLI images for the study area before and after atmospheric correction.

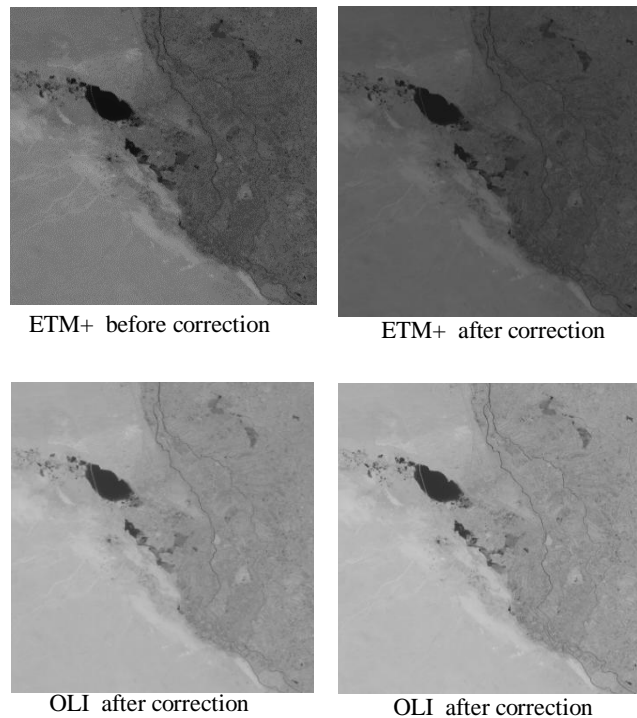


Fig.7: Illustrates the atmospheric correction effects on processed Landsat images.

IV. Prediction Models Of ETM+ From OLI

The difference between the ETM+ and OLI reflectance because of the 8-days difference in the Landsat-7 and Landsat-8 satellite passes over the study area will be reduced by implementing the following prediction methods.

A. Linear-Regression Relationship

This prediction method was introduced by (Neil Flood., 2014). It takes the reflectance values from OLI image, adjust them to be more like ETM+ reflectance, and then use those in models which were originally fitted to ETM+ data. The relationship used to predict the ETM+ image band reflectance ρ_{ETM+} from the equivalent reflectance band of the OLI image ρ_{OLI} is given by;

$$\rho_{ETM+} = C_0 + C_1 \rho_{OLI} \quad (3)$$

Where: C_0 and C_1 are linear regression coefficients.

B. Cross-Correlation-Factor Relationship

In this prediction method, pair of bands of ETM+ images are used, one before and another after the predict time of the equivalent $OLI_{(band\ of\ predict\ time)}$ band [i.e. $ETM+_{(band\ before)}$ and $ETM+_{(band\ after)}$], to determine the cross-correlation-factor, given by [7];

$$r = \frac{ETM+_{(band\ after)} - OLI_{(band\ of\ predict\ time)}}{OLI_{(band\ of\ predict\ time)} - ETM+_{(band\ before)}} \quad (4)$$

The predict band of $ETM+_{(predict)}$ can now estimate, using;

$$ETM+_{(predict)} = \frac{ETM+_{(band\ after)} + r \times ETM+_{(band\ before)}}{1 + r} \quad (5)$$

Fig.8 shows the predicted ETM+ bands using the linear regression and cross-correlation relationships.

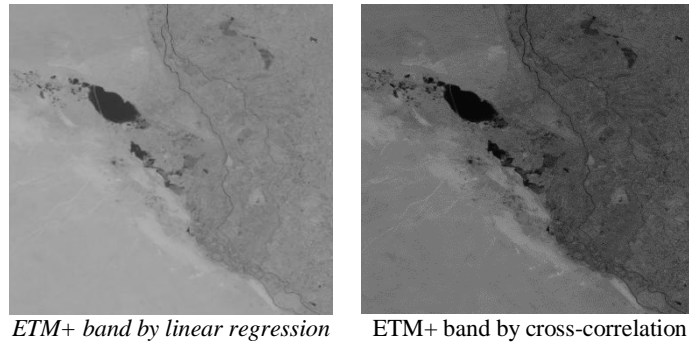


Fig.8: Corrected ETM+ images by linear regression and cross-correlation relationships.

V. Scatterplot Classification Method

It is well known that the soil has property which shows a linear relationship between the near-infrared “NIR” and the visual red “VR” reflectance bands. The length of the linearity between the “NIR” and “VR” responses is affected by the soil’s dryness or wetness contents [8]; i.e. it is shortened for homogenous soils, and extended as the soil’s contents varies.

Therefore, as the soil line is defined, the corresponding reflectance regions of the other spectral classes can be decided accordingly. This phenomenon has been adopted by [9] to introduce a new classification technique based on the scatterplot between the “VR” and “NIR” bands, as illustrated in Fig.9.

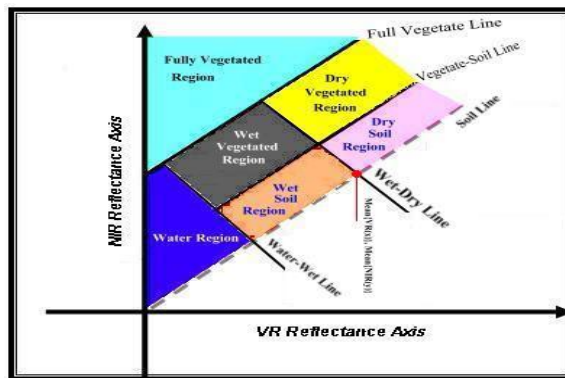
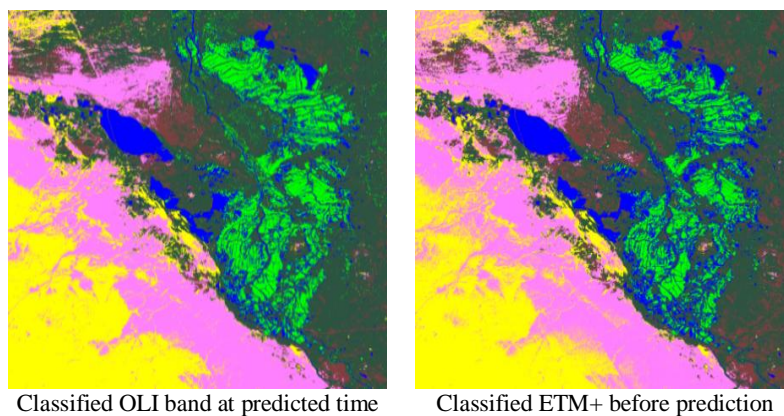


Fig.9: Classification Scheme Based on Scatterplot.

This classification method will be utilized to determine the Landcover percentage components in study area images with concentration on the vegetated zones. Fig.10 shows the classified image bands of ETM+ before and after the prediction operations (using the linear-regression and the cross-correlation), compared with equivalent OLI bands at the predicted time.



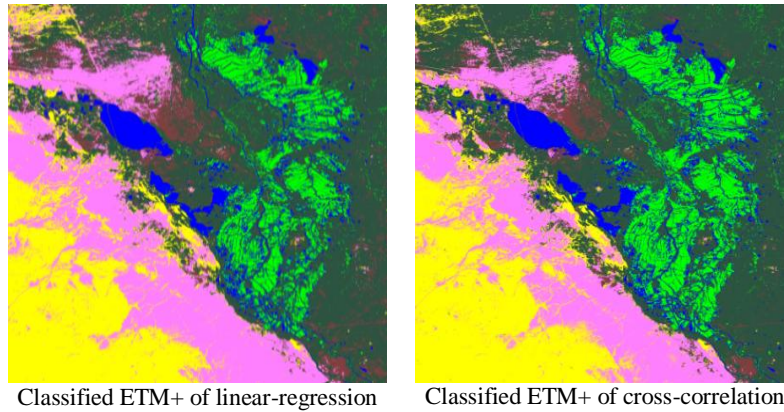


Fig.10: Classified OLI and ETM+ images before and after the calibration processes

VI. Results And Discussions

Implementing the linear-regression on $ETM+_{band3}$ and the equivalent OLI_{band4} , and $ETM+_{band4}$ with its equivalent OLI band OLI_{band5} , the regression coefficients C_0 and C_1 have been determined, given in Table-2.

Table-2: Regression coefficients for TOA reflectance of ETM+ and OLI equivalent bands

Band	C_0	C_1
ETM 3 & (OLI 4)	0.015	0.857
ETM 4 & (OLI 5)	0.01	0.758

Fig.11 represents the scatterplot chart between the corresponding bands of table-2.

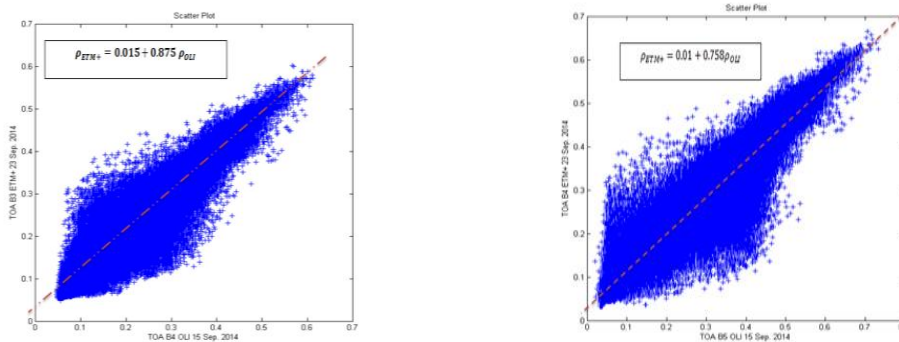
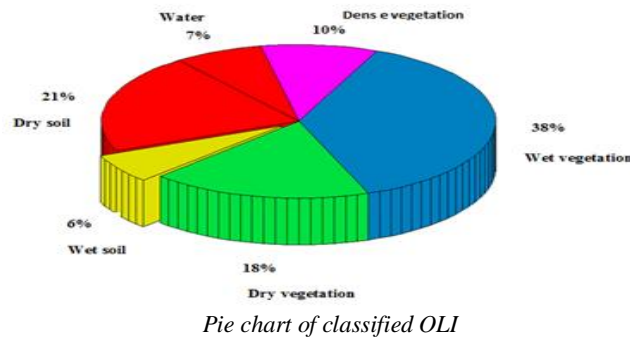


Fig.11: Scatterplots between atmospherically corrected equivalent bands of ETM+ and OLI images.

For the purpose of convergence verification between the predicted $ETM+$ and OLI bands, using the linear-regression model, Fig.12 the classified versions of the OLI band and the $ETM+$ bands before and after the prediction operation.



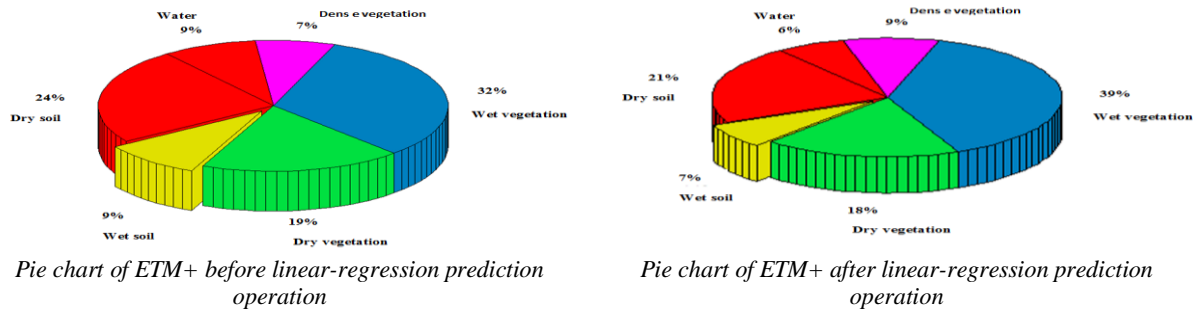


Fig.12: Illustrates the convergence of Landcover components between the classified OLI and ETM+ images by implementing the linear-regression operation.

For the cross-correlation-factor model, as described in Eqs.(4&5), pair of ETM+ bands was required to make the predicted ETM+ band converge to the equivalent OLI band of specific time. For examples ETM+ bands (3&4), captured at 7&23Sept 2014 were used to predict the ETM+ band match with the equivalent OLI bands (4&5) captured at 15Sept. 2014. Fig.13 shows the scatterplot drawn between the predicted *ToA* bands of ETM+ images with the *ToA* OLI bands (4 & 5) captured at 15Sept.2014.

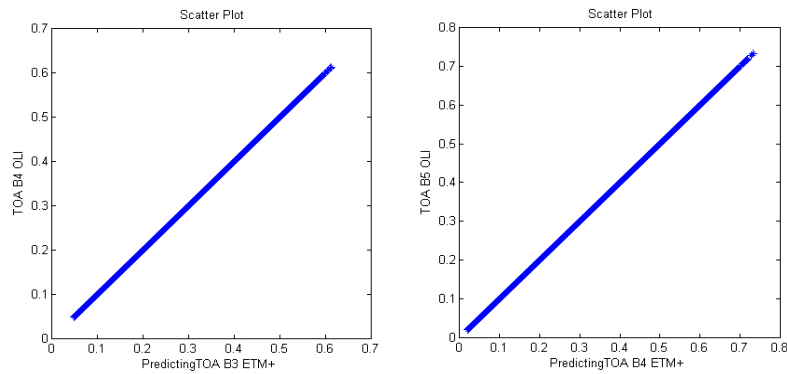
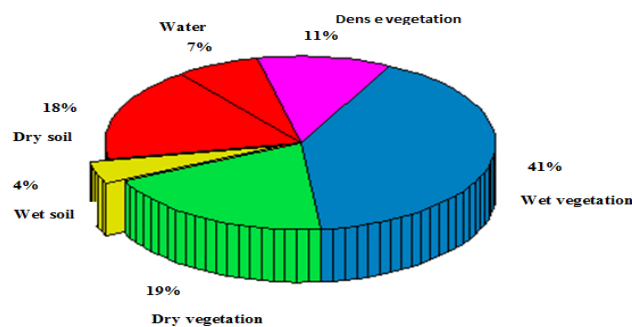


Fig.13: Scatterplots between the predicted ETM+ *ToA* bands and the OLI *ToA* bands captured at 15 Sept.2014.

Once again, for the purpose of convergence confidence, the predicted ETM+ band is classified by the scatterplot classification method to be compared with the OLI classified band shown in Fig.12, illustrated in Fig.14.



Pie chart of calibrated ETM+ by cross-correlation method

Fig.14: The Pie chart of the calibrated ETM+ image by using the cross-correlation-factor method.

Finally, the percentages of the Earth's surface components have been computed for the OLI and ETM+ classified image bands and listed in Table-3.

Table-3: The percentages of the Landcover Earth's surface components in the classified bands of ETM+ and OLI images for the study area

Sensor	dry soil	wet soil	dry veg.	wet veg.	dense veg.	water
OLI 15 Sep.	21%	6%	18%	38%	10%	7%
ETM+ 23Sep.	24%	9%	19%	32%	7%	9%
ETM+ 7Sep.	25%	9%	18%	31%	5%	11%
ETM+ Predicating Model A	21%	7%	18%	39%	9%	6%
ETM+ Predicating Model B	18%	4%	19%	41%	11%	7%

VII. Conclusions

The time difference in the Landsat satellites (7 &8) passes over a specific area is eight days. Because the core of the current study is estimating the yield of agricultural crop which greatly depend on the vegetative growth of plants that is rapidly change in such a period of time, so the current research adopted two different calibration techniques to remove the differences in the images that were captured by the different satellites. Both the Landsat-7 (ETM+) images and the Landsat (OLI) images have been firstly corrected to remove the atmospheric reflectance effects. The corrected images then calibrated chronologically to reduce the changes resulted from difference of satellite passage over the study area. The linear-regression and the cross-correlation models have adopted and modified to achieve the desired purpose. For the purpose of verification of the convergence of the processed images, the classification method that is based on the scatterplot between the visible red (VR) and the near-Infrared (NIR) bands is used to determine the percentage rates of the Landcover components in the images of the study area. The results showed that the cross-correlation-factor model was better than the linear-regression model. This cross-correlation method was previously proposed to harmonize normal difference vegetation index (NDVI) images; here we have modified it to deal with normal satellite image bands.

References

- [1] P. Teillet, J. Barker, B. Markham, R. Irish, G. Fedosejevs, and J. Storey, Radiometric cross-calibration of the Landsat-7 ETM+ and Landsat-5 TM sensors based on tandem data sets . Remote Sens. Environ, 39–54, 2001.
- [2] A.E. Boloorani, Multi- Source Remotely Sensed Data Combination: Projection Transformation Gap-Fill Procedure. Sensors, 8, 4429-4440, 2008
- [3] J. Irons, J. Dwyer, and J. Barsi, The next Landsat satellite: The Landsat data continuity mission. Remote Sens. Environ. 122, 11–21, 2012
- [4] S.M. Ali, Gap-Filling Restoration Methods for ETM+ Sensor Images, Iraqi Journal of Science, Vol.54, No.1, 206-214, 2013
- [5] D.A. Lee, Two Algorithms for Constructing a Delaunay Triangulation, International Journal of Computer and Information Sciences, Vol. 9, No. 3, 219-242, 1980
- [6] G.M. Chander, Summary of current radiometric calibration coefficients for Landsat MSS, TM, ETM+, and EO-1 ALI sensors. Remote Sensing of Environment 113, 893–903, 2009
- [7] N. Flood, Continuity of Reflectance Data between Landsat-7 ETM+ and Landsat-8 OLI, for Both Top-of-Atmosphere and Surface Reflectance: A Study in the Australian Landscape, Remote Sens., 6, 7952-7970, 2014
- [8] Xu. Dandan, Compare NDVI extracted from Landsat 8 imagery with that from Landsat 7 imagery, American Journal of Remote Sensing, 2(2), 10-14. 2014
- [9] J. Jensen, Introductory digital image processing, Englewood Cliffs, New Jersey: Prentice-Hall A Division of Simon & Schiter, 1986
- [10] S.M. Ali, New Fully Automatic Multispectral Image Classification based on Scatterplot Method, International Journal of Emerging Technology and Advanced Engineering, Volume 3 , Issue 10, 388-394. 2013.